The frequency dependence of compressional wave velocity and attenuation coefficient of intertidal marine sediments

G. B. N. Robb, A. I. Best, J. K. Dix, and J. M. Bull
National Oceanography Centre: Southampton, European Way, Southampton, SO14 3ZH, United Kingdom

T. G. Leighton and P. R. White
Institute of Sound and Vibration Research, University Road, Southampton, SO17 1BJ, United Kingdom

(Received 15 September 2005; revised 6 July 2006; accepted 2 August 2006)

To advance the present understanding of the frequency dependence of compressional wave velocity and attenuation in marine sediments a series of well-constrained *in situ* acoustic transmission experiments (16 to 100 kHz) were performed on intertidal sediments. The processing techniques incorporated *in situ* spreading losses, sediment to transducer coupling and thorough error analyses. Significant variations in velocity and attenuation were observed over scales of tens of meters within the same sediment type. Velocity was generally nondispersive in sands, while highly variable silt velocities prevented any meaningful dispersion estimates from being determined. The attenuation coefficient was proportional to frequency for 75% of the experimental sites. The measured compressional wave properties were compared to predictions from the Grain-Shearing model. For the sandy sites, the phase velocities predicted by the Grain Shearing model exceed those measured, while predicted phase velocities agreed with measured group velocities at specific locations for the silty sites. For both silts and sands predicted dispersions are comparable to the intrinsic errors in group velocity and hence undetectable. The attenuation coefficients predicted by the Grain Shearing model adequately describe the measured attenuation coefficients, within the observed variability.
 [DOI: 10.1121/1.2345908]

PACS number(s): 43.30.Ma, 43.20.Hq, 43.20.Ye [RAS] Pages: 2526–2537

I. INTRODUCTION

A wide range of commercial and academic marine disciplines, from oil and gas surveying[1] to marine archaeology,[2] require knowledge of the geotechnical properties of the seafloor. The inversion of geoacoustic properties obtained through remote refraction/reflection profiling represents a promising approach for obtaining these *in situ* geotechnical properties for large volumes of seafloor sediment. Conversely, marine sonar applications require accurate predictions of the geoacoustic properties of seabed sediments, in order to enhance object detection through active sonar techniques. In order to perform the inversions/predictions required for these applications, the frequency dependencies of the more commonly used compressional wave properties need to be determined accurately for a range of sediment types. Although there is a long history of good work in this field, the diversity of sediment types and the wide range of frequencies of interest means that further measurements are required to determine the frequency dependencies and to refine theories.

In situ transmission tests offer a compromise between laboratory and remote techniques, and therefore present a promising manner of examining the frequency dependence of compressional wave velocity and attenuation coefficient in marine sediments. A highly flexible experimental geometry allows the compressional wave properties of a well-defined volume of sediment to be measured over a wide frequency range. Furthermore, the sediment disturbance associated with probe deployment can be minimized through careful consideration of the deployment techniques and experimental geometry adopted.

There are, however, other practical difficulties associated with performing such measurements that have tended to limit the number of published *in situ* compressional wave datasets available, generally to a single sediment type or a single frequency. Although it is clear that the use of data from a single research project, using a single acquisition device and common data processing techniques, are inherently more directly comparable, this lack of data has promoted the use of data compilations to incorporate wider ranges of frequencies and sediment types. In order to generate data, which allows generic frequency-dependent relationships to be examined, it is important that the repeatability of the acoustic signal emitted by the source is quantified, a factor that will depend on both the coupling of the transducers to the sediment and the electronic signal transmitted to the source. Some processing techniques also require that corrections for spreading losses are applied, and while the assumption that spreading losses are the same in water and sediment is approximately true in some cases, the use of *in situ* spreading losses would be more relevant.

These experiments utilized a single data acquisition system and enhanced data processing techniques to measure both compressional wave velocity and attenuation coefficient, with corresponding intrinsic errors. The frequency range investigated, i.e., 16 to 100 kHz, spans those used by sub-bottom profilers and those incorporated by laboratory techniques. The frequency dependence of these properties

TABLE I. A summary of published research on velocity dispersion in marine sediments, with **N** denoting no dispersion and velocities expressed in terms of the velocity of water ν_w, where absolute values are not available. A lack of published information is indicated by a dash.

Frequency (kHz)	Velocity	Degree of dispersion	Sediment type	First author and reference
14–100	1704–1712 m s^{-1}	**N**	*In situ* sand	Hamilton (Ref. 5)
15–1500	$1.189 \cdot \nu_w$	**N**	Reconstituted sand/silt/clay	McLeroy (Ref. 6)
0.2–4.7	1410–1740 m s^{-1}	**N**	*In situ* silt	Best (Ref. 7)
375–935	1560–1741 m s^{-1}	**N**	Sand/silt/clay samples	McCann (Ref. 8)
25–100	1727–1797 m s^{-1}	4%	*In situ* sand	Buckingham (Ref. 9)
0.125–400	$1.05 \cdot \nu_w$–$1.17 \cdot \nu_w$	11.4%	*In situ* sand	Williams (Ref. 10)
50–350	-	0.5%	Reconstituted sand	Wingham (Ref. 11)
3–200	$0.93 \cdot \nu_w$–$0.99 \cdot \nu_w$	4%–6%	Artificial silt/clay	Hampton (Ref. 12)
20–100	-	25 m s^{-1}	*In situ* sand	Gorgas (Ref. 13)
1–30	1580–1720 m s^{-1}	8.9%	*In situ* sand	Turgut (Ref. 14)
0.125–50	1580–1755 m s^{-1}	11.1%	*In situ* sand	Stoll (Ref. 15)

were examined using empirical fits, while the validity of the grain-shearing model[3,4] was investigated.

II. PRESENT UNDERSTANDING OF COMPRESSIONAL WAVE PROPERTIES

There is still contention over the frequency dependence of both compressional wave velocity and attenuation coefficient in marine sediments. A significant volume of literature exists to support both nondispersive[5–8] and dispersive[9–15] relationships (see Table I). Doubt has been expressed as to the applicability of laboratory based studies to *in situ* values[6,8,11,12] (owing to sediment disturbance), while the large variations in velocity dispersion observed by different studies (0.5% to 11.4%) highlights the need for a series of experiments that examines a large range of sediment types and frequencies in a well-constrained manner. Also, error analyses presented in earlier pioneering works generally refer to the standard deviation arising from variability. As the field matures, it is necessary to examine instead the intrinsic error associated with the experimental and processing techniques adopted.

The frequency dependence of compressional wave attenuation coefficient α (in dB m^{-1}) is typically expressed using

$$\alpha = k_A f^q, \tag{1}$$

where k_A is the constant of proportionality[5] and q is the exponent of frequency, f. Published measurements of compressional wave attenuation coefficients in marine sediments are presented in Table II. Though a number of researchers report an attenuation coefficient that is proportional to frequency[5,6,16–20] from 40 Hz to 1.5 MHz, there is some concern over this relationship for a number of reasons. These are namely the deviation from unity of certain published exponents of frequency[5,17,20] or a lack of statistical validation.[16,18,19] The difficulty of reliably determining the frequency dependence of the attenuation coefficient is highlighted by a compilation of data from fine-grained sediments.[21] Although this presents an optimum exponent of 1.12, it is stated that, within 95% confidence limits, it is impossible to distinguish between this optimum exponent and an exponent of unity. Finally, attenuation coefficients measured at low frequencies[22,23] (5 to 250 Hz) are less than those predicted by the linear extrapolation of higher frequency data,[5] hence implying that the frequency dependence of attenuation coefficient may differ in this low frequency range. Attenuation coefficients that do not vary with frequency in a linear manner are observed by a number of authors.[7,9,12,21,24–27] Alternative data compilations observe "some evidence" for nonlinear frequency dependence, with nonlinear regions occurring between 10 and 100 Hz in sands and 1 to 10 kHz in silts.[23]

III. *IN SITU* EXPERIMENTS

A series of well-constrained *in situ* acoustic transmission experiments were performed on inter-tidal sediments along the south coast of England. These experiments utilized a new acoustic probe system, the Sediment Probing Acoustic Detection Equipment (SPADE).[28] The SPADE consists of a source and a pair of matched receivers (Fig. 1) that were deployed individually in aluminium channels. The use of a fixed rig, which may allow the relative positions of the probes to be more accurately defined, was declined, owing to the associated reduction in the flexibility of the system. The source consists of a section of piezoceramic material with a convex emitting face. This operates in an untuned manner over the usable frequency range of 16 to 100 kHz, while the matched receivers possess sensitivities of −189 to −198 dB *re* 1 V/μPa over this range. The waveforms selected for the transmission experiments consisted of a series of tonal pulses,[28,29] each possessing 10 cycles modulated by a Blackman-Harris envelope[30] with central frequencies from 16 to 100 kHz, in 2 kHz increments. Signals emitted by the SPADE are repeatable to the sampling period of ±1 μs and ±3.2% in amplitude, while water tests and field trails confirmed that received signals accurately resemble shifted, scaled versions of the voltage signals sent to the source transducer.[29]

TABLE II. Summary of published research on the frequency dependence of a compressional wave attenuation coefficient in marine sediments, including measured attenuation coefficients, exponent q of frequency dependence, and sediment type. A lack of published information is indicated by a dash.

Frequency (kHz)	Attenuation coefficient (dB m^{-1})	Exponent q	Sediment type	First author and reference
3.5–100.0	0.6–74.3	0.94–1.1	*In situ* sand to clay	Hamilton (Ref. 5)
15–1500	-	1	Reconstituted silt/clay	McLeroy (Ref. 6)
25–100	8–60	Nonlinear	*In situ* sand	Buckingham (Ref. 9)
0.125–400	1–200	Nonlinear	*In situ* sand	Hampton (Ref. 12)
3.5–100	1.5–55	1	Compilation of data (sands)	Hamilton (Ref. 16)
4–50	0.28–3.00	1±15%	*In situ* Mud	Wood (Ref. 17)
0.04–0.09	0.59	1	*In situ* clayey silt	Bennett (Ref. 18)
5–50	0.30–1.86	1	*In situ* silty clay	Lewis (Ref. 19)
5–50	-	1.00–1.26	*In situ* sand	McCann (Ref. 20)
0.03-500	5.6×10^{-4}–90	1.12	Compilation of data (muds)	Bowles (Ref. 21)
0.05–1.00	2.2×10^{-4}–9.5×10^{-4}	1.25–1.50	-	Evans (Ref. 24)
20–40	0.10–2.48	0.6–3.4	Sand to clayey silt samples	Shumway (Ref. 25)
100–1000	40–150	1.3–2.0	Silt and clay core samples	Courtney (Ref. 26)
20–300	3–34	Nonlinear	Glass beads	Hovem (Ref. 27)
0.2–4.7	0–4	Nonlinear	*In situ* silt	Best (Ref. 7)

The present project chose to examine intertidal sediments only, as this allowed the positions and orientations of the probes to be measured as accurately, and more easily, than would have been possible for a similar deployment in completely submerged sediments. This, however, introduces the risk of encountering partially saturated sediments. Gas bubbles can be introduced into marine sediment through a variety of mechanisms (e.g., the anaerobic decomposition of organic matter[31]) and have been observed in both intertidal sediments[32] and wholly submerged sediments.[33] Until 2003, bubbles with radii less than 500 μm could not be resolved by the present bubble sizing techniques available, namely, the x-ray CT scanning of pressurized cores.[34] Therefore published *in situ* acoustic measurements from "saturated" sediments have assumed full saturation.

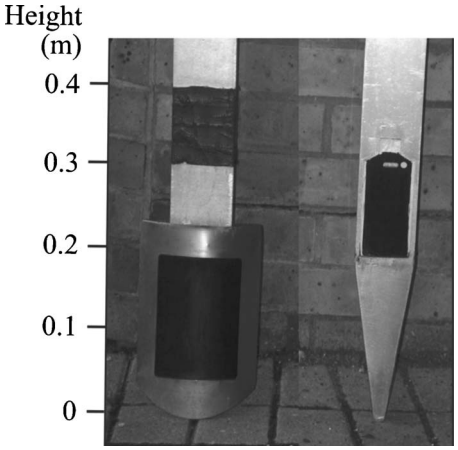

FIG. 1. SPADE source (left) and receiver (right), both inserted in aluminium channels to assist their deployment into the sediment.

In order to allow the attenuation coefficient of the sediment to be measured, it was essential that the beam patterns associated with the SPADE are known. The receiver's beam pattern[28] varies from an almost omnidirectional field at 1 kHz to a much more directional field at 100 kHz. The relatively simple geometry of the transmission experiments allowed estimated changes in the amplitude of the received signal, which arise from the receiver orientations, to be incorporated into the intrinsic error budget (Sec. IV).

The pressure field emitted by the source was modeled using a modified version of a technique used to predict spreading losses for circular array transducers.[35] This considered the source to be a segment of a cylinder from which sound radiates outward, which was subdivided into a two-dimensional (2-D) grid of elements (Fig. 2). The manipulation of Eq. (10) in Borsboom *et al.*[35] results in the following expression for the pressure at a field-point X and angular frequency ω:

$$P(X,\omega) = W(\omega)\cdot dx\cdot dy\sum_{n=1}^{N_1}\sum_{m=1}^{N_2}\frac{e^{-i\omega R'/v}\cdot e^{-i\omega R_{n,m}/v}}{2\pi R_{n,m}}, \qquad (2)$$

where $W(\omega)$ is the spectrum of the selected voltage pulse; dx and dy are the size of the elements in the x and y directions, respectively; N_1 and N_2 are the number of integration steps in each direction; $R_{n,m}$ is the distance from source element n,m to field point X; and R' is the minimum distance between point X and the transducer surface. The pressure response at field-point X associated with a given frequency ω can be

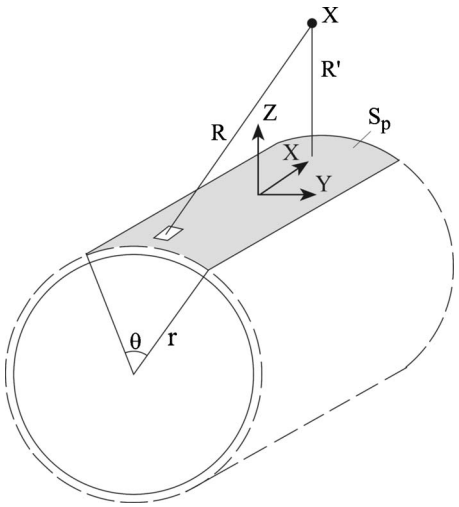

FIG. 2. Geometry used in the simulation of the pressure field emitted by the source, denoted by the shaded area segment S_p. An example field point X is displayed, along with the distance R from source element dS, the minimum distance to the source R', the parameters defining the source (r and θ) and the coordinate system used. From Borsboom *et al.* (Ref. 35).

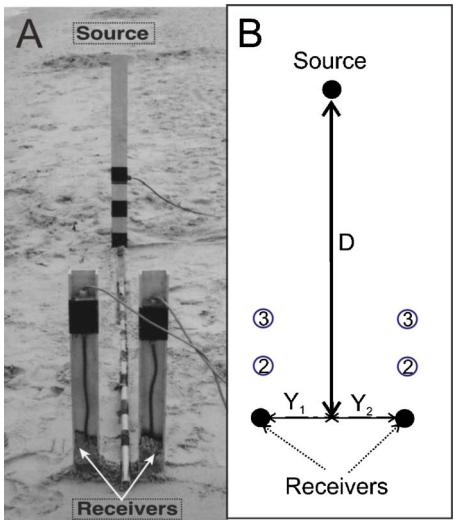

FIG. 3. SPADE deployment during fieldwork, with image (a) of receivers positioned at approximately the same S-R separation, lying on either side of the central line marked by the measuring pole. Diagrammatic plan view (b) displays measured perpendicular distance, D, and offsets, Y_1 and Y_2, to receivers, with subsequent receiver deployments indicated at positions 2 and 3. In order to clearly display the offsets, the plan view has been rescaled, with offsets used in the fieldwork ranging from 1 to 10% of the S-R separations used.

obtained from the temporal maximum of the inverse Fast-Fourier Transform of $P(X,\omega)$. The pressure field was computed for the horizontal plane that intercepts the center of the source, as the use of a common depth for source and receivers in the fieldwork performed ensured that all receiver deployments lie in this plane. Deviations from this common depth are incorporated into the error budget (Sec. IV).

The model was verified through calibration signals measured using the SPADE source and receivers in a water tank.[29] Transmitted signals were detected by placing the receivers in the horizontal plane that intercepts the center of the SPADE source. The goodness of fit between the observed and modeled decay ranged from 0.79 and 1.00, representing a good to excellent fit. Discrepancies between the predicted and measured decays lay within the error limits in the experimental setup, i.e., ±2° in the horizontal angle, ±1° in the vertical angle, ±0.02 m in source-receiver (S-R) separation, and ±0.01 m in depth. Hence, the pressure model described above adequately predicts the pressure emitted by the SPADE source in nondispersive media.

Pressure fields were simulated for pulses with central frequencies from 16 to 100 kHz (in increments of 2 kHz) and compressional wave velocities from 1300 to 1800 m s^{-1} (in increments of 100 m s^{-1}), i.e., the range of velocity values obtained from field data analysis. Near-to-farfield transitions were computed as the distance from the center of the source to the last axial maximum.[36] These lay less than 0.43 m from the source for all compressional wave velocities measured and all frequencies used.

The experimental procedure involved inserting the source and a pair of receivers vertically into the sediment, with the inclination of the probes to the vertical accurate to ±2°. The two receivers were deployed at approximately the same S-R separation astride the perpendicular to the source face (Fig. 3). While the experimental/processing techniques adopted herein only require a single source and receiver, the use of two receivers increased the quantity of data that could be collected. The center of the source and receivers were placed at a common depth of 1 m (±0.02 m), which reduced the possibility of interfering arrivals from seabed surface reflections, while allowed sediment samples to be readily obtained from the sediment volume through which the acoustic wave propagated. The receivers were positioned at approximately the same S-R separation, with S-R separations calculated from the measured perpendicular distances, D, and offsets, Y_1 and Y_2 [see the plan view in Fig. 3(b)]. S-R separations varied from 1.0–8.1 m, all of which were located in the farfield. A series of acoustics pulses were transmitted, consisting of 5 shots at each central frequency from 16 to 100 kHz (in increments of 2 kHz). The receivers were removed and redeployed at a closer S-R separation before the same series of acoustics pulses was transmitted. The successive use of closer S-R separations ensured that previous deployments did not disturb sediment that later deployments would reexamine. Tidal windows allowed the examination of between three to seven S-R separations at each location.

In the silts, the source and receivers could be deployed through the manual application of a vertical force to the top of the aluminium channels. In the sands this was not possible and hence a modified box corer (width 0.13 m and breadth 0.21 m) was used. This was initially inserted in the sediment to a depth of 1 m and the sand within it excavated. The probes were then inserted and, after the removal of the box corer, the sediment refilled. This allowed the majority of sediment through which the acoustic pulses propagates to remain undisturbed, with the range of disturbed sediment around each probe (<0.1 m) much less than the S-R separations examined.

To minimize the risk of encountering unsaturated sediments, sites were selected to lie in coastal regions of the United Kingdom with relatively low tidal ranges (i.e., less

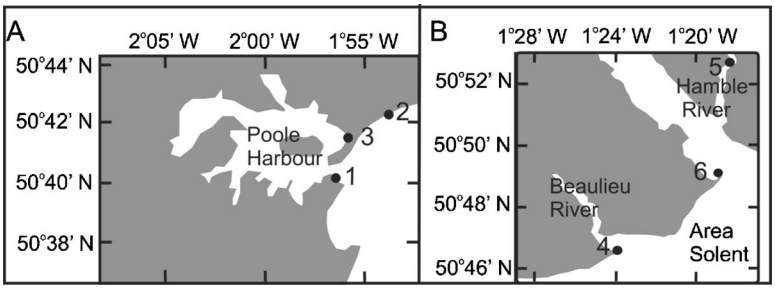

FIG. 4. Geographical location of the intertidal sites examined, including (a) three sandy sites (Sites 1 – 3) and (b) three silty sites (Sites 4 – 6) used in this study. Grey regions denote land.

than 1.5 m). Six sites were examined in total, including three sand sites (Sites 1–3) located at the mouth of Poole Harbour [see Fig. 4(a) and Table III] and three silt sites (Sites 4–6) located in Southampton Water and the Beaulieu estuary [see Fig. 4(b) and Table III]. At each site between two and four specific locations were examined in order to allow any natural sediment variability to be assessed.

At each location sediment samples were collected from a depth of 1 m and the temperature and salinity of the pore water was recorded (see Table IV). The grain size distribution at each site was obtained from between 6 to 12 sediment samples collected from the insonified sediment volume. In addition, a single push core was collected from each site, from which porosity was measured at 1 cm intervals along the core using a multisensor core logger.[37] The geotechnical properties are presented in Table III, which quotes mean values with standard deviations. The sediments were classified using standard sedimentological procedures[38,39] as medium to fine sands, with porosities from 29.3%–34.5%, and coarse to medium silts, with porosities from 63.2%–80.1%. Although great care was taken to select visually uniform sites the actual variabilities in mean grain diameter M varied from 0.07 to 0.35 ϕ for sandy sites and 0.15 to 0.30 ϕ for silty sites. Larger scale heterogeneities, such as shells, shell fragments, and pebbles with diameters from 2 mm to 10 cm, were observed at Sites 1, 2, and 4.

IV. DATA PROCESSING TECHNIQUES

Established acoustic transmission processing techniques were adapted to both assess the repeatability of the transducer to sediment coupling and to incorporate the sound pressure fields directly relevant to the sediment type under examination. In the present section we summarize these techniques, with the reader referred to Robb *et al.*[28] for a more detailed discussion. Any deviations from assumptions used by these processing techniques were accounted for through the error analysis employed.

Common preprocessing steps[28] were applied to both the voltage signals sent to the source transducer and the received signals. While the majority of received signals resembled shifted, scaled versions of the voltage signals sent to the source transducer with negligible distortions (Fig. 5), some distorted waveforms were detected. These were attributed to the presence of interfering signals, arising from scatter from sediment heterogeneities and reflections from the sediment surface, and were omitted from the following analysis.

The technique adopted to calculate the group velocity of the sediment optimized data from a range of S-R separations. Arrival times t_A were obtained from a correlation of the ana-

TABLE III. Geotechnical properties of the six intertidal sites examined, including geographical location, sediment type, mean grain diameter M (ϕ), porosity n (%) and clay, sand and silts fractions (%). The ϕ scale (Ref. 39) is defined by $M(\phi)=-\log_2[M(mm)/M_0]$, where M_o represents a "standard" grain diameter of 1 mm.

Site	Location	Sediment type	Mean grain diameter M(ϕ)	Porosity n(%)	Sand (%)	Silt (%)	Clay (%)
1	N 50° 40' 42-47" W 001°56' 56-58"	Mod well sorted Bimodal medium sand	1.58±0.35	29.3±1.0	99.8±0.3	<0.2	<0.2
2	N 50° 42' 23-29" W 001° 54' 29"	Well sorted Unimodal medium sand	1.84±0.15	32.9±2.5	99.0±0.3	<1.0	<1.0
3	N 50° 41' 00-43" W 001°55' 54-55"	Well sorted Unimodal fine sand	2.16±0.07	34.5±1.7	99.6±0.3	<0.4	<0.4
4	N 50° 46' 39" W 001°23' 43-45"	Poorly sorted Unimodal medium silt	6.75±0.30	80.1±2.8	7.7±1.5	81.0±3.3	10.7±3.2
5	N 50° 52' 34-35" W 001° 18' 43-44"	Poorly sorted Unimodal medium silt	6.77±0.20	60.5±2.1	7.6±4.5	82.0±2.9	9.2±3.5
6	N 50° 48' 56" W 001°18' 34"	V. poorly sorted Unimodal coarse silt	5.31±0.15	63.2±0.9	27.5±7.0	69.7±6.5	2.8±0.4

TABLE IV. Pore water properties at sand and silt sites examined, including salinity (S), temperature (T), density, and bulk modulus.

Sites	Salinity $S(0/00)$	Temperature T (°C)	Density (kg m^{-3})	Bulk modulus (GPa)
Sandy (1–3)	0.3–6.3	14–18	999–1003	2.26–2.29
Silty (4–6)	0.3–30.4	7–11	1000–1023	2.09–2.23

lytical received signal with the analytical voltage signal sent to the source transducer. These arrival times are related to the S-R separation d, the group velocity ν and a constant time lag associated with SPADE t_L through

$$t_A = d/\nu + t_L. \tag{3}$$

The group velocity at each frequency was therefore obtained from the reciprocal of the gradient of a linear least-squares fit between arrival time and S-R separation. The total error in arrival time, t_E, was calculated by combining the intrinsic timing error in the digital acquisition card (± 1 μs) with the error introduced through the use of analytical signals at the correlation stage (± 10 μs) in quadrature.[28] This allowed the standard deviation in velocity σ_V, which was adopted as the relevant error, to be computed from

$$\sigma_V = \sqrt{t_E^2/N(\overline{d^2} - \overline{d}^2)}, \tag{4}$$

where N is the number of data points to which the linear fit is applied and the overscore notation denotes the statistical mean.[40] The intrinsic errors for the dataset examined ranged from ± 20 to ± 70 m s^{-1} in sands and ± 10 to ± 25 m s^{-1} in silts.

The technique developed to calculate attenuation coefficient incorporates both the spreading losses relevant to the sediment under examination and the effects of variable transducer to sediment coupling in the error analysis. The received pulse was resampled to 10 MHz and the signal amplitude $A(f,d)$ assigned the value of the maximum peak-to-peak voltage. The resulting amplitude is a function of the following processes:

$$A(f,d) = V_O(f) \cdot S_T(f) \cdot G(f,d) \cdot R_T(f) \cdot R_e(f) \cdot C \cdot e^{-\alpha_n(f)d}, \tag{5}$$

where spreading losses $G(f,d)$ are a function of frequency f and S-R separation d. The amplitude of the voltage signal transmitted to the source $V_O(f)$, the Transmit Voltage Response of the source transducer $S_T(f)$, the response of the receiving transducers $R_T(f)$, the electronic gain of the receiving amplifiers $R_e(f)$, and the attenuation of the sediment in nepers m^{-1} $\alpha_n(f)$ are all functions of frequency, while the coupling term C is considered constant[28] at each location examined. The comparison of the received signal amplitudes at a single frequency, correction for spreading losses using simulated sound pressure fields applicable to the sediment under examination (see Sec. III), and taking natural-logarithms reduces Eq. (5) to

$$\ln(A_C) = B_1 - \alpha_n d, \tag{6}$$

where A_C represents the amplitudes with spreading losses accounted for and B_1 is a constant. Hence, at each location and frequency, a weighted linear least-squares fit was to applied to $\ln(A_C)$ against d, the gradient of which is equal to the effective attenuation coefficient α_n in nepers m^{-1}.

Intrinsic errors[28] in attenuation coefficient were computed by combining errors arising from the resolution of the acquisition card; the variability of the coupling parameter; the use of pressure fields computed at discrete velocities only; and uncertainties in the measured gain of the receiving amplifiers. For the magnitude of the received amplitudes observed (5.7 mV to 10 V), the error associated with coupling variability represents the dominant element. The approximate error in each value of $\ln(A_C)$, Δ, was obtained from

$$\Delta = A_e/A_C, \tag{7}$$

where A_e is the resulting error in A_C. Hence, the error in the attenuation coefficient, σ_α, was obtained from

$$\sigma_\alpha = \sqrt{\frac{\overline{\overline{\Delta}}}{N(\overline{\overline{d^2}} - \overline{\overline{d}}^2)}}, \tag{8}$$

where a double overline denotes a weighted mean.[40] The resulting intrinsic errors ranged from ± 1 to ± 7 dB m^{-1} for all sites examined.

This approach cannot be used without first checking the effect of neglecting the asymmetry of the errors in Δ, an inherent omission arising from the use of symmetric errors in corrected amplitudes. Such analysis of the data showed that the attenuation coefficients obtained using asymmetric errors and those obtained using the approach above differ by less than 0.07 dB m^{-1}, while errors in attenuation coefficient[28] differ by less than 17.5%.

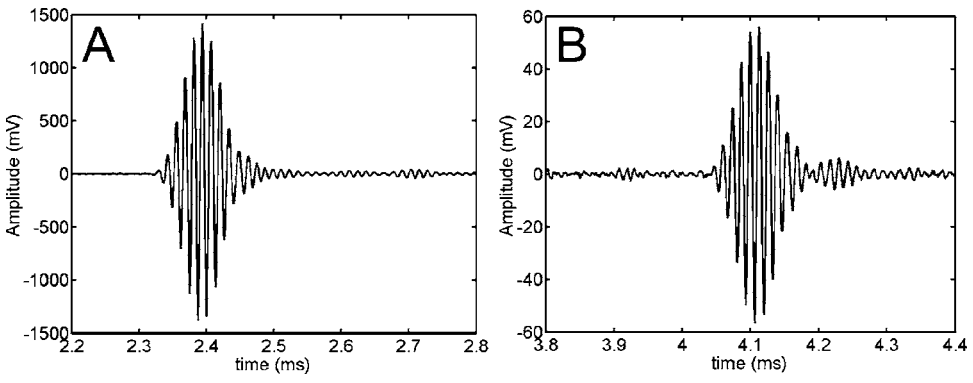

FIG. 5. Example waveforms received at Site 6 (Location 2) with central frequencies of 80 kHz and S-R separations of 2.51 m (a) and 5.00 m (b).

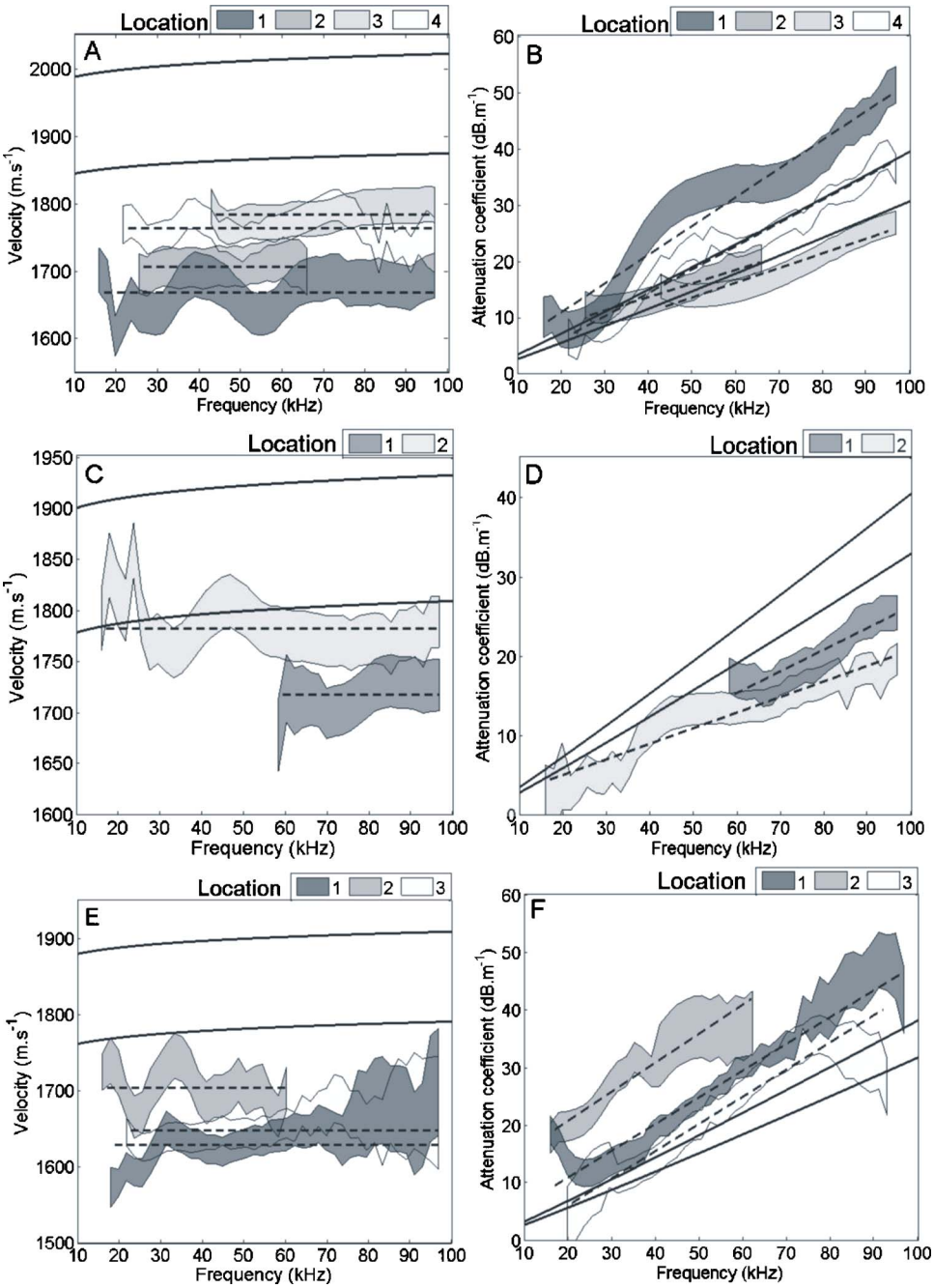

FIG. 6. Compressional wave properties of intertidal sandy sites including velocities for Sites 1 (a), 2 (c), and 3 (e) and attenuation coefficients for Sites 1 (b), 2 (d), and 3 (f). The measured group velocities and attenuation coefficients, with intrinsic errors, are denoted by shaded regions (see legends for specified locations). For each location the weighted mean of velocity and weighted least-squares fit to attenuation coefficient are displayed by dashed lines. The limits of the phase velocities and absorption coefficients predicted by the G-S model are denoted by solid lines.

V. EXPERIMENTAL RESULTS

The compressional wave velocities and attenuation coefficients are displayed in Fig. 6, for predominantly sandy sites (Sites 1 to 3), and Fig. 7, for the predominantly silty sites (Sites 4 to 6). In these figures, data at certain frequencies and locations have been omitted, where distorted waveforms resulted in insufficient degrees of freedom for the application of the linear fits (see Sec. IV).

The common frequency dependencies presented in the literature for velocity and attenuation coefficient were tested for their applicability to these intertidal sites. They include the hypotheses that compressional wave velocity is independent of frequency,[16] and that both compressional wave velocity and attenuation coefficient are proportional to frequency.[5] These hypotheses were tested using a weighted mean and a weighted linear least-square fit, respectively.[40] The weighted linear least-square fits are expressed as

$$v = v_A \cdot f + c_1, \tag{9}$$

$$\alpha = k_A \cdot f + c_2, \tag{10}$$

where v_A, and k_A are the constants of proportionality, and c_1 and c_2 are respective values of velocity and attenuation coefficient corresponding to a frequency of zero. Note that Eq. (10) is a modified version of Eq. (1), with $q=1$. The inclusion of the term c_2 accounts for the possibility of a nonlinear relationship between the attenuation coefficient and frequency outside the frequency range examined here.

For each hypothesis, the deviation of the measured compressional wave property from a weighted fit was converted

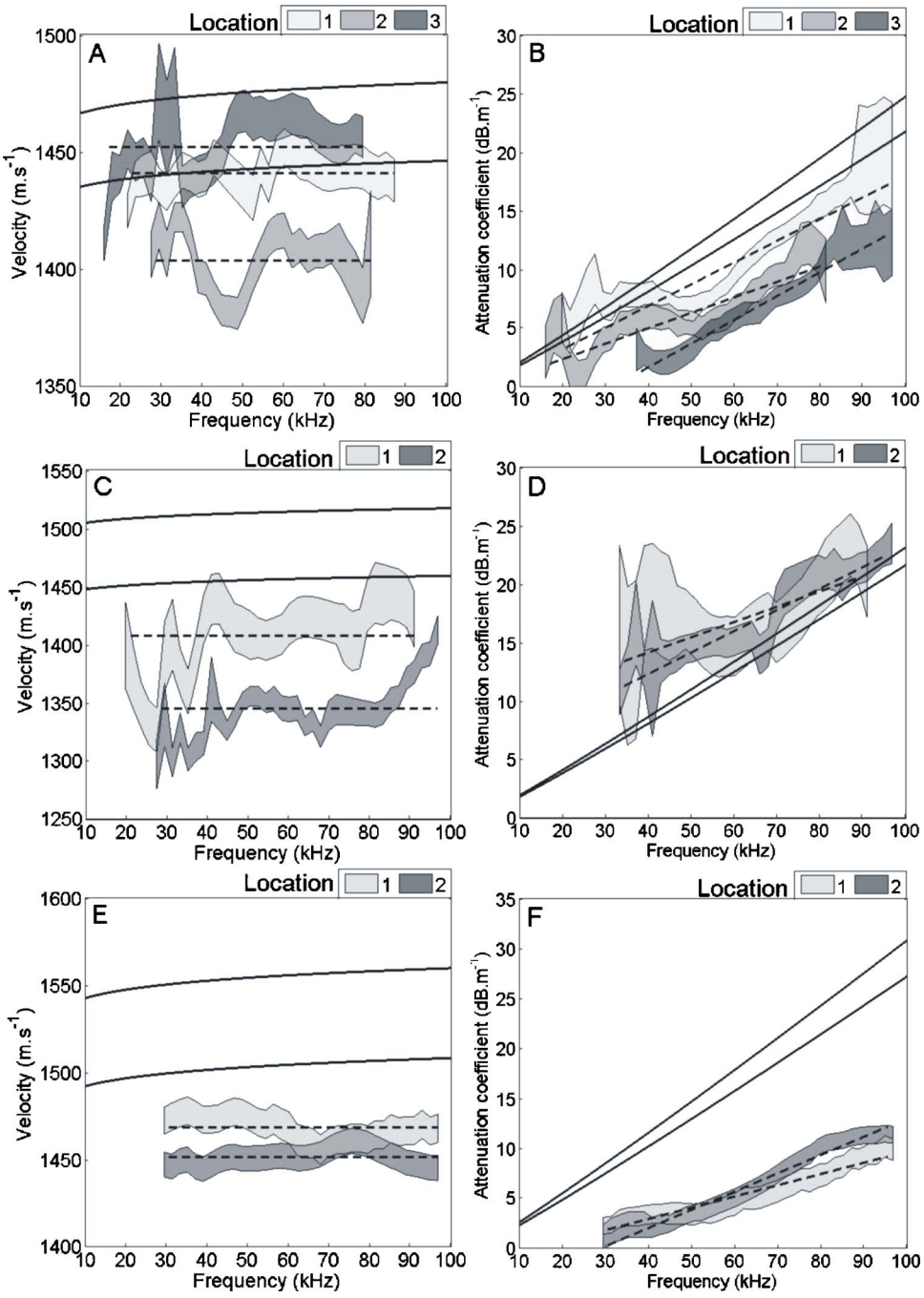

FIG. 7. Compressional wave properties of intertidal silty sites including velocities for Sites 4 (a), 5 (c), and 6 (e) and attenuation coefficients for Sites 4 (b), 5 (d), and 6 (f). The measured group velocities and attenuation coefficients, with intrinsic errors, are denoted by shaded regions (see legends for specified locations). For each location the weighted mean of velocity and weighted least-squares fit to attenuation coefficient are displayed by dashed lines. The limits of the phase velocities and absorption coefficients predicted by the G-S model are denoted by solid lines.

into a confidence limit using the χ^2 distribution.[41] Confidence limits greater than or equal to 95% are considered to indicate an acceptable statistical probability that the weighted fit accurately represents the measured values. The results of the frequency-dependence analysis are displayed in Fig. 6, Fig. 7 and Table V, with standard deviations quoted as the relevant errors. As analysis did not support velocities that were proportional to frequency for either sandy or silty sites (standard deviations in ν_A were greater than ν_A) results from Eq. (9) are omitted from both Table V and the following discussion.

Confidence limits for weighted mean velocities were greater than 95% for seven of the nine predominantly sandy locations. This supports the hypothesis of negligible velocity dispersion from 16 to 100 kHz for these sandy sediments within the observed errors. For the predominantly silty sites, confidence levels in the weighted mean were extremely low for Sites 4 and 5, while nondispersive velocities were supported for Site 6. The velocities at Sites 4 and 5 display a sharply oscillatory nature, particularly at lower frequencies, which conceals any fundamental frequency-dependent trends that may be present. Although the depth at which the probes were deployed (1 m) and the S-R separation used (8.1 m) introduces the possibility of interference from surface reflections for frequencies less than 60 kHz, the omission of distorted waveforms from the analysis (Sec. IV) rules out this interference as a cause of these oscillations. It is more likely that velocities at these sites are dominated by a considerable degree of variability. This argument is supported by the more spatially variable nature (Sites 4 and 5 display relatively

TABLE V. Compressional wave properties of intertidal sites, including the spread of properties at a single frequency; and the results of the frequency-dependent statistical analysis performed (i.e. weighted mean velocity, constant of proportionality for attenuation coefficient k_A and corresponding χ^2 confidence limits).

				Applicability of non dispersive velocity		Applicability of attenuation coefficient proportional to f	
Site	Velocity spread ($m\ s^{-1}$)	Atten. spread ($dB\ m^{-1}$)	Location	mean ($m\ s^{-1}$)	χ^2 Conf. (%)	k_A ($dB\ m^{-1}\ kHz^{-1}$)	χ^2 Conf. (%)
1	130	24.4	1	1668±5	>97.5	0.51±0.02	<80.0
			2	1712±6	>99.5	0.14±0.03	>99.5
			3	1783±5	>99.5	0.27±0.03	>99.5
			4	1760±4	<80.0	0.41±0.01	<80.0
2	128	8.7	1	1718±6	>99.5	0.29±0.04	>99.5
			2	1782±4	>97.5	0.19±0.01	>97.5
3	166	18.6	1	1631±4	>95.0	0.52±0.02	>99.5
			2	1703±6	<80.0	0.50±0.05	>99.5
			3	1647±4	>99.5	0.48±0.03	>95.0
4	85	7.3	1	1440±1	>90.0	0.19±0.01	<80.0
			2	1404±1	<80.0	0.13±0.01	<80.0
			3	1455±1	<80.0	0.20±0.01	>99.5
5	109	6.2	1	1408±3	<80.0	0.13±0.04	>99.5
			2	1345±3	<80.0	0.18±0.01	>99.0
6	31	3.1	1	1469±1	>99.0	0.10±0.01	>99.5
			2	1451±1	>99.5	0.17±0.02	>99.5

large variabilities in the mean grain diameter; see Table III) and a more heterogeneous nature (shells were observed at Site 4) of these sediment volumes.

The statistical analysis indicates that, from 16 to 100 kHz, attenuation coefficient is proportional to frequency for both sandy and silty sediments, with confidence limits greater than the threshold value of 95% for three quarters of the locations examined (Table V). Constants of proportionality k_A are greater in sands than in silts, ranging from 0.14 to 0.52 $dB\ m^{-1}\ kHz^{-1}$ (with errors less than ±0.05 $dB\ m^{-1}\ kHz^{-1}$) in the sands and 0.1 to 0.2 $dB\ m^{-1}\ kHz^{-1}$ (with errors less than or equal to ±0.04 $dB\ m^{-1}\ kHz^{-1}$) in the silts.

For comparison purposes, the velocities were converted to velocity ratios, using pore water velocities (1425 to 1483 $m\ s^{-1}$) computed[29] from salinities and temperatures measured at the experimental sites (Table IV). Velocity ratios varied from 1.06 to 1.26 (±1.1 to ±4.5%) at the sandy sites, and 0.92 to 1.04 (errors less than ±1.9%) at the silty sites. While these values broadly agree with velocity ratios published by Richardson *et al.*[42] (0.98 to 1.12 for subtidal medium sands to clays), the velocity ratios for the silts extend below those previously measured. This may be a consequence of the presence of free-gas bubbles in the silts, which may be introduced by either the intertidal nature of the sediments or the biogenic decomposition of organic material (Total Organic Contents ranged from 3% to 11% in the silts). The effect of free gas on the compressional wave velocity depends on the relationship between the insonifying frequencies and the resonant frequencies of the bubbles.[43,44] At frequencies less than resonance, the velocities of partially saturated sediments are less than those of saturated sediments, while at frequencies greater than resonance the velocities of partially saturated and saturated sediments are approximately the same. Of direct relevance to this work are previous *in situ* measurements of compressional wave velocities in partially-saturated beach sands,[32] which recorded velocity ratios as low as 0.09 for frequencies of 800 Hz. The much higher velocity ratios observed in the present project indicates that either the frequencies examined in this project (16 to 100 kHz) are approximately equal to or greater than the resonance frequencies or the sediments examined in this project possess extremely small fractions of gas bubbles.

Attenuation coefficients ranged from 2 to 52 $dB\ m^{-1}$ at the sandy sites and 1 to 23 $dB\ m^{-1}$ at the silty sites, values that agree with previously published results for subtidal sediments over a similar frequency range.[9,21] The variability of geoacoustic properties was examined using the maximum range of velocities and attenuation coefficients spanned by a single frequency (see Table V). The sandy sites possessed the greater variability than the silty sites, particularly for an attenuation coefficient. Unfortunately this could not be related to porosity changes, owing to the collection of a single push core from each site, while no correlation was observed with the observed variability in the mean grain diameter.

VI. MODELING OF *IN SITU* COMPRESSIONAL WAVE PROPERTIES

The measured *in situ* compressional wave properties were compared to those predicted by the grain-shearing (G-S) model.[3,4] The G-S model[3,4] considers marine sediments to act as unconsolidated granular media and considers a new type of dissipation arising from grain-to-grain contacts, which has fundamentally different properties to the more classical dissipation mechanisms of viscosity or Coulomb friction.[45] This intergranular dissipation allows elastic type behavior to arise from intergranular interactions rather than finite frame moduli.

In order to predict the phase speed and attenuation coefficient of the two waves supported (one compressional and one shear), the G-S model requires 14 geotechnical input parameters and frequency.[4] For certain parameters, only generic site-independent values could be determined. A nominal depth of 1 m was used, while the rms grain roughness was evaluated from porosity versus mean grain diameter regression equations presented by Buckingham.[4] The parameters describing the microscopic interactions at grain boundaries, namely the compressional and shear coefficients and strain-hardening index, cannot be measured. These are typically obtained through fitting the G-S model to measured compressional and shear properties at a known porosity, mean grain diameter and depth (which become the reference porosity, mean grain diameter, and depth, respectively). This model fitting step requires the knowledge of at least three of the four acoustic properties predicted by the theory, i.e., compressional and shear phase velocities and attenuation coefficients. As only two parameters have been measured for the intertidal sediments under consideration, this step cannot be undertaken. Hence the compressional and shear coefficient, strain-hardening index and reference porosity, mean grain diameter and depth that are used in the present implementation of the G-S model are taken from previously published implementations of the G-S model, values that can be considered to be fixed for all siliciclastic sediments.[4]

For the remaining parameters, a range of input values could be determined for each site examined and therefore the limits of predicted velocities and attenuations could be predicted for each site. *In situ* measured values were used for porosities and mean grain diameters (see Table III), while the properties of the fluid, namely bulk modulus and density, were determined from measured salinities and temperatures using the standard equations of state[46] (see Table IV). The densities and bulk moduli of the grains were obtained from the literature,[29] with densities ranging from 2650 to 2750 kg m^{-3} and bulk moduli ranging from 32 to 49 GPa.

The compressional wave properties predicted by the G-S model are displayed in Figs. 6 and 7 for the sandy and silty sites, respectively. For the sandy sites the phase velocities predicted exceeded those measured. Predicted dispersions were less than 1.7% (<35 m s^{-1}), both of which are comparable to the intrinsic errors in group velocity and are therefore undetectable. Measured attenuation coefficients were adequately described, within the observed variability, by the predicted attenuation coefficients (2.6 to 40.5 dB m^{-1}).

It is interesting to note that the compressional wave velocities predicted by Wood's Equation[47] for a suspension agrees more closely with measured velocities than those predicted by the G-S model (for the relevant range of physical parameters compressional wave velocities predicted by Wood's Equation range from 1700 to 1821 m s^{-1} for Site 1, 1629 to 1780 m s^{-1} for Site 2, and 1619 to 1738 m s^{-1} for Site 3). This indicates that the values presented for the compressional and shear coefficients for subtidal sands[4] overpredict normal and tangential stresses associated with intergranular sliding that are present in the intertidal sediments examined in the present project. The difference in these stresses between subtidal and intertidal sediments can be postulated to be due to the different processes that govern the supply, deposition, and dynamics of the sediment in each environment.

For the silty sites the predicted phase velocities (1435–1559 m s^{-1}) agree well with measured velocities at Site 4 and tend to overestimate measured group velocities at Sites 5 and 6. Dispersions are 1.1% (17 m s^{-1}), which are either less than or comparable to the intrinsic errors in group velocity ($<\pm 25$ m s^{-1}) and hence undetectable. Attenuation coefficients predicted by the G-S model vary from 1.8 to 30.8 dB m^{-1} for the frequency range examined. These broadly agree with measured attenuation coefficients at Sites 4 and 5 and overestimate measured attenuation coefficients at Site 6.

While the agreement between measured and predicted attenuations implies that the loss mechanism incorporated by the G-S theory is applicable to both sandy and silty sediments, it is interesting to consider the effects of additional scattering losses. It is unlikely that Rayleigh scattering from sediment grains is a significant source of energy loss, as the smallest wavelength examined (16 mm) was much greater than the maximum grain diameter encountered (<1 mm). This is supported by the observation that Rayleigh scattering is only significant for frequencies greater than 500 kHz in sands[10] with mean grain diameters of approximately 414 μm (1.27ϕ), i.e., coarser than those examined within this project. Any additional scattering losses present are more likely to arise from larger scale scattering centers or spatial variability in the sediment across the insonified volumes (see Sec. III).

VII. CONCLUSIONS

In this work we focused on ascertaining the frequency dependence of compressional wave velocity and an attenuation coefficient in marine sediments over the frequency range 16 to 100 kHz. This was achieved through a series of well-constrained *in situ* transmission experiments performed in intertidal sediments. The processing techniques adopted incorporated *in situ* spreading losses, a quantitative assessment of coupling and waveform variability, and a thorough error analysis.

The compressional wave velocity ratios ranged from 1.06 to 1.26 (± 1.1 to $\pm 4.5\%$) at the sandy sites and 0.92 to 1.04 ($<\pm 1.9\%$) at the silty sites. Attenuation coefficients ranged from 2 to 52 dB m^{-1} at the sandy sites and 1 to 23 dB m^{-1}, with intrinsic errors less than ± 7 dB m^{-1}. A significant variability was observed in both the velocity and attenuation coefficient between the measurement locations, which are separated by tens of meters in geologically homogenous sediments. This suggests that acoustic propagation measurements made over distances on the meter-to-decimeter scale could be difficult to translate to the average seabed acoustic properties of a larger area. The sandy sites possessed greater variability than the silty sites, particularly in the case of an attenuation coefficient.

An analysis of the common frequency dependencies observed in the literature indicated that, from 16 to 100 kHz, velocity was nondispersive for the majority of the sandy locations examined. For the silty locations, the frequency de-

pendency of velocity was more difficult to ascertain, with nondispersive velocities only supported at Site 6. This is attributed to the more spatially variable and heterogeneous nature of the silty sites concealing any fundamental frequency-dependent trends present. The attenuation coefficient was found to be proportional to frequency from 16 to 100 kHz for both sand and silt sediments, within confidence limits of 95%, for three-quarters of the locations examined.

The grain-shearing (G-S) model was applied as detailed in Buckingham.[4] For the sandy sites the phase velocities predicted by the G-S model exceed those measured. This indicates that the stresses associated with intergranular sliding differ between the subtidal and intertidal environment, a possible consequence of the different processes that govern the supply, deposition, and dynamics of the sediment in each environment. For the silty sites, the predicted phase velocities agree with measured group velocities at specific locations. For both silts and sands, predicted dispersions are comparable to the intrinsic errors in group velocity and hence undetectable. The attenuation coefficients predicted by the G-S adequately describe the measured attenuation coefficients, within the observed variability. Finally, it should be noted that the validation of the geoacoustic models examined has been considerably impaired by the variability of the measured velocities and attenuation coefficients.

ACKNOWLEDGMENTS

This work was funded by the United Kingdom Natural Environmental Research Council (Grant No. NER/S/A/2000/03621) and the Engineering and Physical Sciences Research Council (Grant No. EP/D000580/1). Thanks are extended to and those who granted permission for site access, namely The National Trust, English Nature, Poole Borough Council, Poole Harbour Commission, The Beaulieu Estate, George Korab, and the management of Mercury and Universal Marinas (Hamble River, Hampshire). Thanks to Andy Harris and James Riggs for the development of the SPADE. For fieldwork assistance we also thank Ronan Apprioual, Stephanie Arnott, Phil Cole, Caroline Cooil, John Davies, Simon Dean, Martin Gutowski, and Robin Saunders.

[1]R. E. Sheriff and L. P. Geldart, *Exploration Seismology* (Cambridge University Press, Cambridge, 1995).
[2]J. M. Bull, R. Quinn, and J. K. Dix, "Reflection coefficient calculation from marine high resolution (Chirp) data and application to an archaeological case study," Mar. Geophys. Res., **20**, 1–11 (1998).
[3]M. J. Buckingham, "Wave propagation, stress relaxation and grain-to-grain shearing in saturated, unconsolidated marine sediments," J. Acoust. Soc. Am. **108**, 2798–2815 (2000).
[4]M. J. Buckingham, "Compressional and shear wave properties of marine sediments: Comparisons between theory and data," J. Acoust. Soc. Am. **117**, 137–152 (2005).
[5]E. L. Hamilton, "Compressional-wave attenuation in marine sediments," Geophysics **37**, 620–646 (1972).
[6]E. G. McLeroy and A. DeLoach, "Sound speed and attenuation, from 15 to 1500 kHz, measured in natural seafloor sediments," J. Acoust. Soc. Am., 1148–1150 (1968).
[7]A. I. Best, Q. J. Huggett, and A. J. K. Harris, "Comparison of *in situ* and laboratory acoustic measurements on Lough Hyne marine sediments," J. Acoust. Soc. Am., **110**, 695–709 (2001).
[8]C. McCann, "An investigation of the acoustical properties of natural materials," Ph.D. thesis, Department of Physical Oceanography, University College of North Wales, 1967.
[9]M. J. Buckingham and M. D. Richardson, "On tone-burst measurements of sound speed and attenuation in sandy marine sediments," IEEE J. Ocean. Eng. **27**, 429–453 (2002).
[10]K. L. Williams, D. P. Jackson, E. I. Thoros, D. Tang, and S. Schock, "Comparison of sound speed and attenuation measured in a sandy sediment to predictions based on the Biot theory of porous material," IEEE J. Ocean. Eng. **27**, 413–428 (2002).
[11]D. J. Wingham, "The dispersion of sound in sediment," J. Acoust. Soc. Am. **78**, 1757–1760 (1985).
[12]L. D. Hampton, "Acoustic properties of sediments," J. Acoust. Soc. Am. **42**, 882–890 (1967).
[13]T. J. Gorgas, R. H. Wilkens, S. S. Fu, L. N. Frazer, M. D. Richardson, K. B. Briggs, and H. Lee, "In situ acoustic and laboratory ultrasonic sound speed and attenuation measured in hererogeneous soft seabed sediments: Eel River shelf, California," Mar. Geol. **182**, 103–119 (2002).
[14]A. Turgut and T. Yamamoto, "Measurements of acoustic wave velocities and attenuation in marine sediments," J. Acoust. Soc. Am. **87**, 2376–2383 (1990).
[15]R. D. Stoll, "Velocity dispersion in water-saturated granular sediment," J. Acoust. Soc. Am., **111**, 785–793 (2001).
[16]E. L. Hamilton, "Acoustic properties of sediments," in *Acoustics and the Ocean Bottom*, edited by A. Lara-Saenz, C. Ranz-Guerra, and C. Carbo-Fite (Cosejo Superior de Investigaciones Cientificas, Madrid, 1987), pp. 4–58.
[17]A. B. Wood and D. E. Weston, "The propagation of sound in mud," Acustica **14**, 156–162 (1964).
[18]L. C. Bennett, "*In situ* measurements of acoustic absorption in unconsolidated sediments," Trans., Am. Geophys. Union, **48**, 144 (1967) (abstract only).
[19]L. F. Lewis, "An investigation of ocean sediments using the deep ocean sediment probe," Ph.D. thesis, Department of Ocean Engineering, University of Rhodes Island, 1971.
[20]D. M. McCann and C. McCann, "The attenuation of compressional waves in marine sediments," Geophysics **34**, 882–892 (1969).
[21]F. A. Bowles, "Observations on attenuations and shear wave velocity in fine-grained marine sediments," J. Acoust. Soc. Am. **101**, 3385–3397 (2000).
[22]R. D. Stoll, "Marine sediment acoustics," J. Acoust. Soc. Am., **77**, 1789–1799 (1985).
[23]A. C. Kibblewhite, "Attenuation of sound in marine sediments: A review with emphasis on new low frequency data," J. Acoust. Soc. Am., **86**, 716–738 (1989).
[24]R. B. Evans and W. M. Carey, "Frequency dependence of sediment attenuation in two low-frequency shallow-water acoustic experimental datasets," IEEE J. Ocean. Eng., **23**, 439–447 (1992).
[25]G. Shumway, "Sound speeds and absorption studies of marine sediment by a resonance method," Geophysics **25**, 451–467 (1960).
[26]R. C. Courtney and L. A. Mayer, "Acoustical properties of fine-grained sediments from Emerald Basin: Toward the inversion for physical properties using Biot-Stoll model," J. Acoust. Soc. Am. **93**, 1145–1154 (1993).
[27]J. M. Hovem and G. D. Ingram, "Viscous attenuation of sound in saturated sand," J. Acoust. Soc. Am. **66**, 1807–1812 (1979).
[28]G. B. N. Robb, A. I. Best, J. K. Dix, P. R White, T. G. Leighton, J. M. Bull, and A. Harris, "The measurement of the *in situ* compressional wave properties of marine sediments," IEEE J. Ocean. Eng., in press.
[29]G. B. N. Robb, "The *in situ* compressional wave properties of marine sediments," Ph.D. thesis, University of Southampton, Southampton, 2004.
[30]S. G. Schock, L. R. LeBlanc, and L. A. Mayer, "Chirp sub-bottom profiler for quantitative sediment analysis," Geophysics **54**, 445–450 (1989).
[31]D. D. Rice and G. E. Claypool, "Generation, accumulation, and resource potential of biogenic gas," AAPG Bull. **65**, 5–25 (1981).
[32]R. Bachrach and A. Nur, "High-resolution shallow-seismic experiments in sand, Part 1: Water table, fluid flow and saturation," Geophysics **63**, 1225–1233 (1998).
[33]P. Fleischer, T. H. Orsi, M. D. Richardson, and A. L. Anderson, "Distribution of free gas in marine sediments: a global overview," Geo-Mar. Lett. **21**, 103–122 (2001).
[34]A. H. Reed and K. B. Briggs, "Gas bubbles in marine mud-How small are they?," J. Acoust. Soc. Am. **114**, 2318 (abstract only) (2003).
[35]J. M. G. Borsboom, E. I. Cespedes, A. F. W. Van der Steer, C. T. Lancee, and E. F. Deprettere, "Simulation of circular array ultrasound transducers for intravascular applications," J. Acoust. Soc. Am. **108**, 827–835 (2000).
[36]LE. Kinsler, A. R. Frey, A. B. Coppens, and J. V. Sanders, *Fundamentals in Acoustics* (Wiley, New York, 1982).

[37]A. I. Best and D. G. Gunn, "Calibration of multi-sensor core logger measurements for marine sediment acoustic impedance studies," Mar. Geol. **160**, 137–146 (1999).
[38]G. M. Friedman and J. E. Sanders, *Principles in Sedimentology* (Wiley, New York, 1978).
[39]M. R. Leeder, *Sedimentology: Process and Product* (George Allen and Unwin, London, 1982).
[40]R. J. Barlow, *Statistics: A Guide to the Use of Statistical Methods in the Physical Sciences* (Wiley, Chichester, 1989).
[41]C. F. Dietrich, *Uncertainty, Calibration and Probability* (Adam Hilger, Bristol, 1991).
[42]M. D. Richardson, D. L. Lavoie, and K. B. Briggs, "Geoacoustic and physical properties of carbonate sediments of the Lower Florida Keys," Geo-Mar. Lett. **17**, 316–324 (1997).
[43]A. L. Anderson and L. D. Hampton, "Acoustics of gas bearing sediments I, Background," J. Acoust. Soc. Am. **67**, 1865–1889 (1980).
[44]A. L. Anderson and L. D. Hampton, "Acoustics of gas bearing sediments II. Measurements and models," J. Acoust. Soc. Am. **67**, 1890–1903 (1980).
[45]M. J. Buckingham, "Theory of acoustic attenuation, dispersion, and pulse propagation in unconsolidated granular materials including marine sediments," J. Acoust. Soc. Am. **102**, 2579–2596 (1997).
[46]P. Siedler, "Properties of seawater," in *Numerical data and functional relationships in science and technology*, edited by J. Sunderman (Springer-Verlag, Berlin, 1986), pp. 237–259.
[47]A. B. Wood, *A Textbook of Sound* (G. Bell and Sons, London, 1941).